Photoionization spectrum of H in strong dc electric fields

K. Ng, D. Yao,* and Munir H. Nayfeh

Department of Physics, University of Illinois at Urbana-Champaign, 1110 W. Green Street, Urbana, Illinois 61801

We studied the $m_l = 0$ photoionization channel of H($n = 2$, $m_l = 0$) red and blue states in a dc electric field F theoretically and experimentally in the energy region between the two ionization thresholds: the Stark-induced classical threshold at $E = -2\sqrt{F}$ and the threshold of the field-free atom at $E = 0$. We find that the ionization yield via the "rapidly" ionizing $m_l = 0$ channels concentrates at the two thresholds. Such concentration has not been observed in similar experiments on complex atoms due to a large degree of electron scattering from the ion core that produces significant amounts of mixing among the excitation amplitudes and among the ionization channels. Our results show that the hydrogenic Stark levels of fixed principle quantum number n become sharper as their parabolic quantum number n_1 increases. On the other hand, the levels of fixed n_1 get wider as their quantum number n increases. Moreover, our results show a remarkable property: The ratio of the cross sections from the red and from the blue $m_l = 0$ states of $n = 2$ fall on a universal curve when plotted as a function of Z_1, the fraction of the nuclear charge that drives the bound motion. Also, the ratio is found to be larger than 1 in two regions where $Z_1 = 0 - \frac{1}{4}$ and $\frac{1}{2} - \frac{3}{4}$, less than 1 in the rest of the Z_1 regions, $Z_1 = \frac{1}{4} - \frac{1}{2}$ and $\frac{3}{4} - 1$, and is equal to unity at the common boundaries at $Z_1 = \frac{1}{4}$, $\frac{1}{2}$, and $\frac{3}{4}$, thus indicating special properties of these fractional charges.

I. INTRODUCTION

The study of highly excited atoms in externally applied electric fields has seen vigorous growth in the past two years. The possibility of observing spectroscopic novelties has been the impetus for much of this work, but recent developments show promise for wider application.[1] In this paper we present the photoionization spectrum of the H($n = 2, m_l = 0$) state of atomic hydrogen in the presence of a strong dc electric field in the energy region bounded at lower energies by $E = -2\sqrt{F}$ and at higher energies by $E = 0$, the photoionization threshold. We used selective excitation of distinct charge distributions of the $m_l = 0$ state, either a charge distribution which is highly extended up field, ($m_l = 0$ blue state) or a charge distribution that is highly extended down field ($m_l = 0$ red state). We find that the ionization yield via the "rapidly" ionizing $m_l = 0$ channels (states that ionize in times shorter than 1 μsec) concentrate near the two thresholds.[2,3] Such concentration has not been observed in similar experiments in complex atoms. Moreover, our measurements and calculations show that the hydrogenic Stark levels of fixed principle quantum number n get sharper as their parabolic quantum number n_1 increases. On the other hand, the levels of fixed n_1 get wider as their quantum number n increases.

Our results also show that the ratio of the cross sections from the red and blue $m_l = 0$ states of $n = 2$ has remarkable properties. We find that it is greater than 1 in two regions where $Z_1 = 0 - \frac{1}{4}$ and $\frac{1}{2} - \frac{3}{4}$; less than 1 in the rest of the Z_1 regions, $Z_1 = \frac{1}{4} - \frac{1}{2}$ and $\frac{3}{4} - 1$; and is equal to unity for $Z_1 = \frac{1}{4}$, $\frac{1}{2}$, and $\frac{3}{4}$ where Z_1 is the fraction of the nuclear charge that drives the bound motion. This behavior is found to be universal for all states originating from different n manifolds.

Previously pure parabolic states in hydrogen were prepared in states of high principle quantum number after charge exchange of a beam of protons in a rare gas.[4] All but the specific Stark state sought were quenched using static electric fields. Transitions to higher levels at infrared wavelengths were induced using Doppler and Stark tuning. This technique in the presence of an electric field has been used to make precision measurements of the energies and field ionization rates of some excited Stark states of hydrogen. However, application of this method to the states in the region near $E = 0$ would be very difficult, since it would require a powerful, broadly tunable laser in the infrared region; currently, such lasers are unavailable.

The knowledge of the hydrogenic structure is important for the determination of the nonhydrogenic structure in spite of the drastic differences between them. Recently Fano succeeded in formulating a nonperturbative theory of the Stark effect of nonhydrogenic Rydberg atoms[5] which utilizes (a) hydrogenic wave functions at large distances, and (b) scattering of these wave functions by the ionic core. Parameters of aspects (a) and (b) of a state are calculated separately and then combined analytically. Thus the eigenfunctions of a nonhydrogenic atom are represented by a linear superposition of the hydrogenic Stark wave functions in parabolic coordinates. This mixing affects the distribution of the excitation oscillator strength and the ionization rates in the various energy regions. Such calculations based on the Fano formulation were done by Harmin.[6] The theoretical aspects of photoionization of hydrogen in strong external electric fields were treated by several researchers.[6-9] However, these works did not include the sizable effects of the electric field on the initial excited state of hydrogen because application to complex atoms, where these effects are negligible, was in mind. Recently we used a numerical technique for the calculation of the spectrum of hydrogen in which

we included the effect of the field on the initial excited states, and found that such effects are key to the understanding of the interaction.[10]

II. PREPARATION OF PARABOLIC CHARGE DISTRIBUTIONS OF H($n=2$)

The experimental apparatus was described previously.[11] Here we only describe it briefly. The technique we use utilizes the simultaneous absorption of two photons from a single tunable pulsed laser beam at 243 nm resulting in excitation from $1s$ to $n=2$, and a few percent photoionization of the resulting $n=2$ population. A second pulsed beam at ~ 366 nm excites states near the continuum from the $n=2$ state. The atomic hydrogen source is a modified Wood discharge tube. An atomic beam is formed by effusion from the discharge region through a multicollimator assembly. The atomic beam is directed into the diffusion pumped cell which contains the field plates. One of the plates has a 3×10 mm^2 slot cut into it to allow the passage of ions. Since the presence of the open slot would lead to an unacceptably nonuniform field, a 0.5-mm spacing copper mesh was soldered over the whole surface of the plate. The beam is loosely collimated, but produces a density of about 10^{11} H atoms/cm^3; the background gas pressure is on the order of 3×10^{-5} torr. Ions produced by the radiations are driven by the electric field through the slot in the grounded plate. They travel through a 1-m-long, field-free drift tube which provides mass analysis. This is necessary since molecular impurities are easily ionized by the ultraviolet wavelengths in use. Ions are detected using an 18-stage venetian-blind electron multiplier capable of single ion detection. Under typical experimental conditions, several hundred ions are detected per pulse. The data are collected and analyzed using an LSI-11 computer system. The two beams cross at a distance of 3 mm from the slot. The diameter of the ionizing beam at this intersection is ~ 0.2 mm, thus giving a spread in the kinetic energy of the protons of $\pm 3\%$. Therefore we do not expect the detection efficiency of protons after the 1-m flight to be sensitive to where they were produced in the laser beam.

The transit time t_s of thermal hydrogen across the effective observation region (1.5 mm—half of the width of the slot in the upper plate) plays an important role in the passage of the protons through the slot and hence in the collection of the ionization. The ionization produced by states that ionize very slowly such that $\tau \gg t_s$ where τ is the ionization lifetime of the atom will not be pushed through the slot because the protons are not produced underneath the slot. On the other hand, ionization from states that ionize in time much shorter than t_s will pass through the slot and hence will be accelerated towards the detector. For ionization lifetimes comparable to the transit time, the fraction of ionization that passes through the slot can be estimated from the simplified expression $1 - e^{-t_s/\tau}$. We should note that in the spectrum studied here, only one out of 27 states has a lifetime that is comparable to t_s while the other 26 have $\tau \ll t_s$. Using 1.6×10^3 m/s for the thermal average velocity of hydrogen in the direction parallel to the width of the slot gives

an estimate of 10^{-6} s for t_s.

The optical beams needed for the excitation of atomic hydrogen are produced using a pulsed laser system which consists of an Nd^{3+}:YAG (where YAG represents yttrium aluminum garnet) laser and two dye lasers. A fraction of the second harmonic of the YAG laser at 532 nm is used to pump one of the dye lasers producing a beam at 630 nm, which is frequency doubled to 315 nm by a potassium dihydrogen phosphate (KDP) crystal and then summed with the residual YAG fundamental by a KDP crystal resulting in a beam at 243 nm with a pulse length of about 15 ns, a bandwidth of about 1.5 cm^{-1}, and pulse energies on the order of 10 μJ. The second dye laser produces a beam at about 555 nm which is summed with part of the YAG fundamental to produce a beam with pulse length near 10 ns, bandwidth of 0.6 cm^{-1}, pulse energies of a few tenths of a millijoule, and a wavelength near 365 nm. To cover the wavelength range needed for this experiment, three different dyes had to be used.

Excitation of highly-excited state hydrogen from the ground state was also achieved recently using one-photon excitation of the $2p$, followed by further excitation using another photon at ~ 360 nm.[12] The photoionization spectrum was recorded in the presence of 4.5 kV/cm static electric field.

We have recently studied the effect of the electric field on the H($n=2$) state, and utilized our two-photon process from the ground state to selectively excite different parabolic states.[10] Here we only quote the relevant information and go beyond by determining the charge distributions of the various states. Since we were interested in applying fields larger than 2 kV/cm, we did not include the Lamb shift in our analysis since the Stark shift becomes comparable to it at ~ 0.475 kV/cm and we did not include the much smaller hyperfine structure (~ 178 MHz) since the Stark shift becomes comparable to it at ~ 80 V/cm.[13] Figure 1 gives the Stark splitting of $n=2$ as a
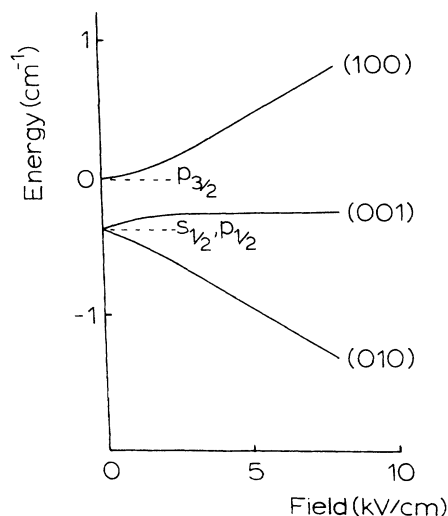

FIG. 1. The splitting of the $n=2$ states vs field including the effects of the fine structure (but ignoring the Lamb shift). The Stark states are labeled at high field by the parabolic states to which they tend.

function of the electric field. At higher fields the states are labeled by their parabolic quantum numbers $(n_1, n_2, |m_l|)$. The state originating from $p_{1/2}, s_{1/2}$ is what we call the $m_l = 0$ red state. The state $(1,0,0)$ originating from $p_{3/2}$ is what we call the $m_l = 0$ blue state. The $|m_l| = 1$ state is the least shifted state.

Figure 2 gives the percentage of purity of the various states if each state is selectively excited by radiation whose effective bandwidth is less than the splittings. Above 10 kV/cm both of the $m_l = 0$ states and the $|m_l| = 1$ state can be purely excited ($> 97\%$). Thus, in principle with fields larger than 8 kV/cm, excitation of pure parabolic states of $n = 2$ in hydrogen can be achieved. But, because our laser bandwidth is ~ 1.5 cm^{-1}, in practice we can only excite pure states using fields larger than 10 kV/cm such that the Stark splitting is larger than 3 cm^{-1}. Since we use quite low atomic hydrogen density, we find no problem in dropping up to 18 kV across our interaction region. In complex atoms, the interaction of the outer electron with the core results in much larger splittings of the various components, thus making the field strength necessary to achieve pure parabolic states in low-lying excited states very high and experimentally not feasible to apply because of electric field breakdown. Of course, the required field strength drops for high-lying excited states. Unfortunately, the wavelengths needed for studies of the photoionization near threshold of these states are out of the range of the convenient optical and infrared tunable sources.

Another important property of the $n = 2$ Stark states which is exploited in our studies is the shape of their charge distributions. Figure 3 gives the charge distribution of the $(1,0,0)$, $(0,1,0)$, and $(0,0,1)$ parabolic states of $n = 2$. The figure shows the x-z cross section through the atom with the nucleus being at the center of the coordinate system. The curves are a line of constant charge density ($\rho = \psi\psi^* = $ const) where the total charge is normalized

FIG. 3. Charge distribution of the parabolic states of $n = 2$ state of hydrogen, (a) is for the blue-shifted $(1,0,0)$ state, (b) is for the unshifted $(0,0,1)$ state, and (c) is for the red-shifted $(0,1,0)$ state. The figure gives a cross section though the atom with the nucleus being at the origin. The contours are lines of constant charge density. The figure shows strong concentration of charge along field and opposite field in (a) and (c). Distances along the axes are measured in atomic units.
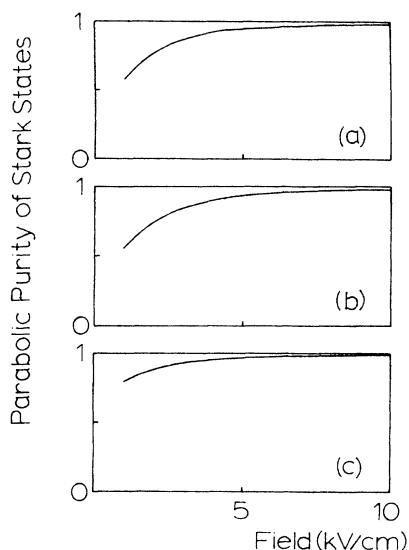

FIG. 2. Purity of the Stark states vs field in terms of their high-field limit parabolic states. (a) is for the blue-shifted 100 state, (b) is for the unshifted 001 state, and (c) is for the red-shifted 010 state.
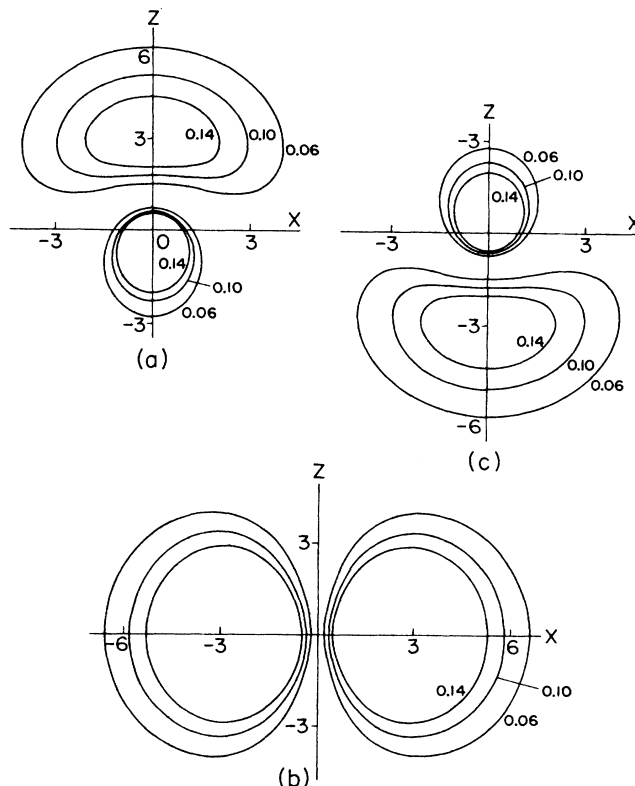
to unity.[13] The large asymmetry in the charge distribution of the $m_l = 0$ blue and red states is quite evident, the concentration being up and down field, respectively. On the other hand, the distribution of the 001 state is symmetric with respect to the field. This figure also shows that the charge distribution of the red and blue states are mirror images of each other when reflected in the $z = 0$ plane. This property is utilized in the present study as a means of probing the shape of the electronic distributions of highly excited Stark states.

III. EXPERIMENTAL RESULTS

Figures 4(a) and 4(b) give the photoionization yield from the $n = 2$, $m_l = 0$ blue state and red state, respectively, as a function of energy in the energy range between $E = -2\sqrt{F}$ and the photoionization threshold at $E = 0$. The electric field imposed is 16.8 kV/cm, and the ionizing laser beam is of π polarization. Each spectrum is taken in four segments with each taking about half an hour in order to avoid drifts in the atomic hydrogen density and because one dye does not cover the whole region. Moreover, each segment is a result averaging five to eight different runs. This procedure, however, may introduce a 2-cm^{-1}
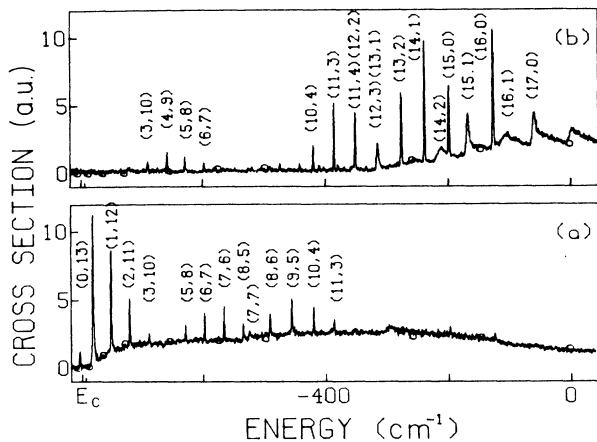
FIG. 4. Experimental photoionization spectra of H($n=2$) at 16.8 kV/cm using π-polarization radiation. (a) is from the excited $m_l=0$ blue state, and (b) is from the excited $m_l=0$ red state.

TABLE I. Absolute calculated photoionization cross section of the smooth spectrum at some selected energies from the $m_l=0$ red and $m_l=0$ blue states at 16.9 kV/cm using π polarization.

| | Cross section (a.u.) | |
Energy (cm^{-1})	Blue state (100)	Red state (010)
-804.16	1.1×10^{-6}	6×10^{-5}
-786.35	6.4×10^{-4}	3.4×10^{-2}
-762.55	4.9×10^{-3}	0.25
-726.73	7.3×10^{-3}	0.46
-653.00	4.15×10^{-2}	0.5
-572.82	8.3×10^{-3}	0.51
-496.38	0.104	0.54
-256.64	0.244	0.58
-145.49	0.43	0.58
0.13	0.53	0.36

systematic shift in the energy scales of various segments relative to each other. There are two aspects of the spectra to be discussed: the sharp Stark peaks and the continuum ionization yield. Let us first consider Fig. 4(a), which gives the ionization yield from the $m_l=0$ blue state. We observe that there is very little activity near and beyond $E=-2\sqrt{F}$ till energies halfway to $E=0$. There we observe that the continuum starts to rise accompanied by the appearance of the sharp Stark peaks. The sharp peaks die out as we approach $E=0$, while simultaneously fairly broad states start appearing near $E=0$.

Figure 4(b), which gives the ionization yield from the $m_l=0$ red state, on the other hand, gives an opposite behavior. We observe that all the ionization activity occurs in the region between the energy $E=-2\sqrt{F}$ and the energy near the halfway point to $E=0$. Just beyond $E=-2\sqrt{F}$ we observe a sharp rise in the underlying continuum accompanied by the appearance of sharp Stark states that die out fairly quickly.

IV. COMPARISON WITH THEORY

We will now compare these results with theory. Several quantum-mechanical numerical calculations have been performed on the effects of a strong electric field on the highly excited states of atomic hydrogen. The calculation of Damburg and Kolosov[8] was concerned with the positions and ionization rates of the states in the combined potential, and did not address the problem of calculating excitation probabilities. Luc-Koenig and Bachelier[9] calculated photoionization cross sections for hydrogen in an electric field, but treated only excitation from the ground state. Harmin's numerical WKB calculation found the cross sections for some excited hydrogenic states; however, since the calculation was performed with a later application to complex atoms in mind, the initial states used were good states of angular momentum (for example, the $3p$ state).[6] Recently we presented a numerical technique for the calculation of the photoionization cross section from individual parabolic states of hydrogen $n=2$ state at

energies near $E=0$ and for positive energies.[10] In here we use the technique to calculate the cross section in the energy range between $E=-2\sqrt{F}$ and $E=0$. Table I gives the calculated cross section of the underlying continuum at a number of selected energies where sharp states do not occur. In order to make direct comparisons we plotted the calculated cross section (open circles) with the experimental results in Fig. 4. The experimental and theoretical cross sections were normalized at a single value of energy (-145.5 cm^{-1}). It is clear from these graphs that the general energy dependence of the cross sections is similar to what we have measured.

We also calculated the cross sections σ, the energies E, and the widths Γ of the sharp Stark states, and identified their quantum numbers (n_1, n_2). Table II gives such information for all cases. First we discuss the positions of the states. Several experimental factors which determine the energy resolution of the experiment need to be considered; they include the bandwidth (1 cm^{-1}), calibration of the dye-laser photon energy and some nonlinearity in the dye-laser scan, and the uncertainty in the measurement of the electric field. An estimate of the latter effect can be made as follows. Since the field is uncertain to about 1%, the energy error from this source is at least 1.0 cm^{-1} for a state shifted by 100 cm^{-1} from its zero-field position. Thus the overall possible energy uncertainty is about 1−2 cm^{-1}; however, because the spectrum was taken in four segments which also involve the change of the dye of the dye lasers, it is apparent from our data that some systematic shifts among the various segments may amount to 2 cm^{-1}. Given this and because there are only a few sharp states, the energy positions for the theoretical and experimental resonances can be matched, and hence the states can be identified.

Since the object of the comparison between the measured and calculated energies is the identification of the peaks, and not a precision test, the level of accuracy is quite sufficient. We clearly state that we do not draw any conclusions from these systematics; they are just experimental errors, and as such it does not serve any purpose to discuss them any further. For precision tests we refer the

TABLE II. Spectroscopic data on the $m_l = 0$ sharp Stark states excited from $n = 2$, $m_l = 0$ blue states using π polarization and in the presence of 16.8-kV/cm dc electric field. These data are the parabolic quantum numbers (n_1, n_2), measured energy E_e, calculated energy E, calculated excitation cross section σ, calculated width (FWHM) Γ, convoluted and measured cross sections $\sigma^{(c)}$ and $\sigma_e^{(c)}$. E, E_e, and Γ are in cm^{-1}; σ, $\sigma^{(c)}$, and $\sigma_e^{(c)}$ are in a.u. For highly asymmetric resonances we have two entries for the widths representing the HWHM on the red and blue sides, unless we cannot measure both due to overlap with nearby states.

(n_1, n_2)	E_e	E	σ	$\Gamma/2$	$\sigma^{(c)}$	$\sigma_e^{(c)}$
(17,0)	-60.72	-57.28	0.67	2.2, 4.6	0.67	0.6
(16,1)	-103.75	-101.50	0.27	10.3[a]	0.27	0.28
(16,0)	-126.46	-123.07	13.64	0.17	2.83	2.2
(15,1)	-167.87	-167.08	0.82	1.7, 2.6	0.82	0.7
(15,0)	-198.54	-196.48	1.2×10^4	3×10^{-4}	3.53	1.25
(14,2)	-210.09	-208.9	0.24	5.7[a]	0.24	0.13
(14,1)	-238.12	-235.06	110.5	0.022	2.95	2.18
(13,2)	-275.88	-274.17	4.5	0.27	1.5	1.28
(13,1)	-314.81	-315.02	0.53×10^6	5×10^{-6}	1.3	
(12,3)	-314.81	-313.58	0.25	1.2, 1.6	0.5	0.33
(12,2)	-351.42	-349.68	1.73×10^4	10^{-4}	2.1	0.95
(11,4)	-351.42	-352.34	0.1	3.0[a]	0.1	
(11,3)	-386.35	-384.35	417.3	0.002	0.63	1.15
(10,4)	-419.23	-419.08	9.45	0.03	0.33	0.35

[a]Unavailable half width because of overlap with other states.

reader to the work of Koch described in Ref. 4.

We now discuss the height of the sharp resonances. Direct comparison between theory and experiment is not possible because the experimental spectrum is actually a convolution of the photoionization cross section as a function of energy with the instrumental response function which we assume to be Gaussian. A source that contributes to the instrumental width is the nonuniformity present in the electric field. If the field is not uniform throughout the interaction volume, the sharp peaks will occur at different energies in different portions of the region leading to a broadening. If the width of the state in question is much smaller than the instrumental bandwidth, then the convolution can be easily worked out; the resonance height would be expected to be reduced by the ratio of its theoretical and instrumental widths Γ/Γ_i. On the other hand, if the width of the state is much larger than the bandwidth of the laser, then its height will not be significantly altered by the finite resolution. For cases where both widths are comparable, the convolution will have to be numerically calculated. We have applied these convolution processes to the theoretical spectrum; the convoluted cross sections $\sigma^{(c)}$ are given in Tables II and III. It has been noted that Tables II and III show some systematic trend in the experimental versus calculated (convoluted) cross sections; whenever $n_1 > n_2$ (especially when significantly larger), the experimental cross sections are larger than the calculated ones. When $n_1 < n_2$, there is no apparent trend. We do not believe that there is any physical significance to such a trend but rather believe that they are just experimental errors.

V. ANALYSIS WITH CHARGE DISTRIBUTIONS

It is interesting to discuss the above results in terms of the charge distributions of the initial and final states. In

TABLE III. Spectroscopic data on the $m_l = 0$ sharp Stark states excited from $n = 2$, $m_l = 0$ red state. The conditions are the same as those of Table II.

(n_1, n_2)	E_e	E	σ	$\Gamma/2$	$\sigma^{(c)}$	$\sigma_e^{(c)}$
(0,13)	-781.64	-782.03	5.29	0.62	3.5	2.2
(1,12)	-751.68	-751.17	5.6	0.25	1.48	1.5
(2,11)	-721.01	-720.27	5.3	0.11	0.79	0.7
(3,10)	-689.07	-689.3	3.01	0.04	0.16	0.18
(5,8)	-629.03	-627.4	63.3	0.002	0.16	0.25
(6,7)	-597.74	-599.4	9.68×10^2	0.003	0.55	0.48
(7,6)	-566.04	-565.24	1.08×10^4	1.5×10^{-5}	0.57	0.55
(6,8)	-566.04	-558.47	0.06	2.1, 3.2	0.06	
(7,7)	-534.8	-523.9	0.188	1.1	0.19	0.25
(8,6)	-490.92	-488.95	0.6	0.38	0.3	0.33
(9,5)	-455.5	-453.95	2.19	0.13	0.38	0.55
(10,4)	-420.0	-419.09	10.03	0.02	0.28	0.43
(11,3)	-386.42	-384.35	50.6	0.002	0.13	0.23

order to do this we utilize the effective potentials of the parabolic ξ and η motion: in the Langer approximation[14] where $m^2 - 1$ is replaced by m^2,

$$V_1(\xi) = -\frac{Z_1}{2\xi} + \frac{m_l^2}{8\xi^2} + \frac{1}{8}F\xi , \tag{1}$$

$$V_2(\eta) = -\frac{Z_2}{2\eta} + \frac{m_l^2}{8\eta^2} - \frac{1}{8}F\eta , \tag{2}$$

where Z_1 and Z_2 are fractions of the nuclear charge that drives the motions, i.e., $Z_1 + Z_2 = 1$. Figure 5 shows these effective potentials in the ξ and η coordinates for $m_l = 0$. The potentials in Fig. 5(a) are for $Z_1 \cong 1$, while those in Fig. 6(b) are for $Z_1 \cong 0$. Inspection of Fig. 5(a) shows that states with $Z_1 \sim 1$ are extended along the ξ axis and compact near $\eta = 0$ ($r = z$); that is, those states extend up the raised barrier in the field direction and are thus raised in energy, or "blue shifted" to the region toward $E = 0$. Inspection of Fig. 5(b), on the other hand, shows that states with $Z_1 \simeq 0$ (i.e., $Z_2 \simeq 1$) are extended along the η axis and compact near $\xi = 0$ ($z = -r$), that is, those states extend in the opposite direction of the field and are thus lowered in energy, or "red shifted" towards the region near $-2\sqrt{F}$.

With the aid of Fig. 3, and using these properties of the distributions, we therefore expect to have large overlaps between the wave function of the $m_l = 0$ blue state of $n = 2$ and those of the $m_l = 0$ blue-shifted states having energies that lie near zero energy when the ionizing laser is of π polarization, while we expect no appreciable overlap between the $m_l = 0$ red state of $n = 2$ and those blue-shifted states near $E = 0$. On the other hand, for the region near $E = -2\sqrt{F}$, we can have red-shifted states originating from high n and blue-shifted states that originate from low n. The overlap of the $m_l = 0$ red state of $n = 2$ with the red-shifted states is expected to be large. Also the overlap between the $m_l = 0$ blue state of $n = 2$ is ex-

pected to be large with the blue-shifted states originating from the low n, however, they do not ionize in this field. This prediction is in agreement with the weak-field results which state that red-to-red or blue-to-blue transitions are much more probable than red-to-blue or blue-to-red transitions. In the weak-field limit, states with $n_1 > n_2$ have their electron predominantly on the positive side of the z axis, and are called blue, while states with $n_1 < n_2$ have their electron predominantly on the negative side of the z axis and are called red. In this study, the field used is not weak and therefore we will examine the region near $n_1 \simeq n_2$ in more detail. To examine this and other features more closely we numerically calculated the ratio of the cross sections from the $m_l = 0$ red and blue states σ_R / σ_B for all the sharp Stark states. Figure 6 shows a plot of these results as a function of the parabolic quantum number n_1 and the principle quantum number n.

First we observe that in the region with n_1 larger than 9, σ_B dominates $\sigma_B \gg \sigma_R$. In the lower-energy region where $n_1 < 9$ we find σ_R dominates, except that in the region near $n_1 = 4$, the domination is disrupted by a deep minimum, thus effectively making σ_R appear to have two separated bunches of sharp peaks. This deep minimum also reflects the appearance of the few isolated states in σ_B near $E = -2\sqrt{F}$. The figure also shows that there are certain states where $\sigma_B \simeq \sigma_R$; these include (10,4), (6,7), (3,10), and (11,4). In these cases we expect the peaks to show simultaneously in Figs. 4(a) and 4(b), indeed they do.

It is also interesting to observe that the general shape of the curve σ_R / σ_B is near universal for the various overlapping manifolds of the principle quantum number n. This is seen in the region of overlap of states corresponding to $n = 13$, 14, and 15, for example. The universality of this curve can be seen much more clearly if one plots the ratio as a function of Z_1 of the states. But before we do that
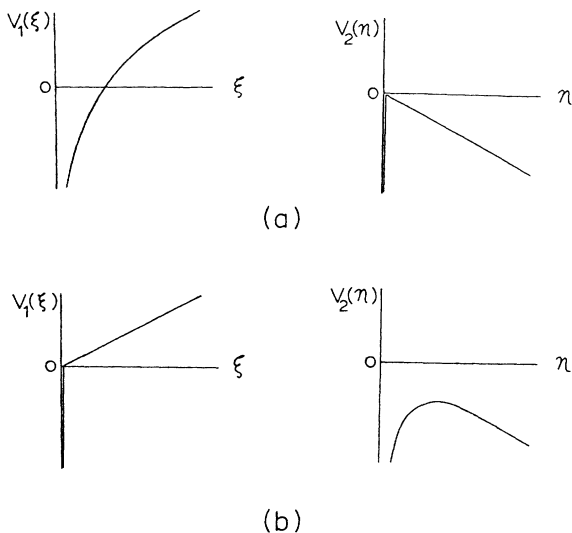

FIG. 5. Effective potentials in the parabolic coordinates ξ and η (a) for a separation parameter value of $Z_l \simeq 1$ and (b) a separation parameter value of $Z_1 \simeq 0$.
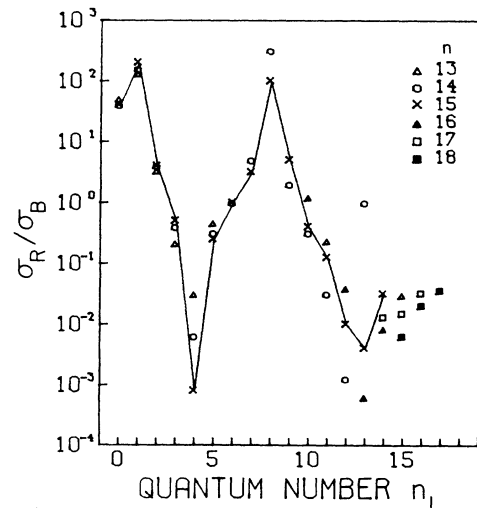

FIG. 6. Ratio of the absolute photoionization cross section from the $m_l = 0$ red state of $n = 2$ (σ_R) and the cross section from the $m_l = 0$ blue state of $n = 2$ (σ_B) using radiation of π polarization, as a function of n_1 and n. The straight lines drawn between the points of the $n = 15$ manifold are just used as a visual aid. The field used is 16.8 kV/cm.

we present a useful curve that plots Z_1 of the various states as a function of their n_1 quantum numbers. Such a relation is plotted in Fig. 7 for various n manifolds. It is worth noting here that different n manifolds give nearly the same dependence for states of low n_1 quantum numbers, and fan out for states of high n_1 with states originating from low n manifolds giving larger Z_1 values.

Figure 8 shows the ratio as a function of Z_1 for the various n manifolds. First of all we observe that the results from the various n manifolds now lie on the same curve, and the variations seen in Fig. 7 disappear. Second, we observe that the fractional charges $Z_1 = \frac{1}{4}, \frac{1}{2}$, and $\frac{3}{4}$ have significant meanings; they demark the regions where the ratio is larger than one and less than one. At these values, however, the ratio is just unity. In fact, the ratio oscillates between larger than unity and smaller than unity as Z_1 is scanned, from low to high values, across these boundaries.

VI. IONIZATION LIFETIMES (RATES)

In this section we examine some aspects of the basic processes via which highly excited states ionize. It should be noted that the energy of a given state and the energy at which classical escape is possible depend on the values of Z_1. In fact, the classical ionization energy is $E_c = -2\sqrt{FZ_2}$. Thus states with different values of Z_2 for the same energy have very different ionization rates depending on how far above or below their energies are their particular ionization limits.

States below their energy for classical escape ionize by tunneling with relatively low rates, while states which are far above E_c ionize very rapidly, leading to broad resonances. In the transitional region near E_c the ionization rate changes rapidly with energy. Since the ionization rate is higher on the high-energy side of the resonance, the resonance in this region is expected to have an extended blue wing.
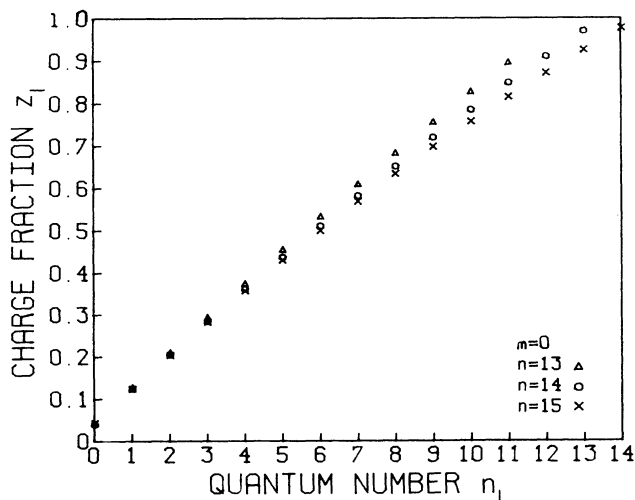

FIG. 7. Fraction of the nuclear charge Z_1 of a given state plotted as a function of the quantum number n_1 of the state for a number of n manifolds, using a field of 16.8 kV/cm.
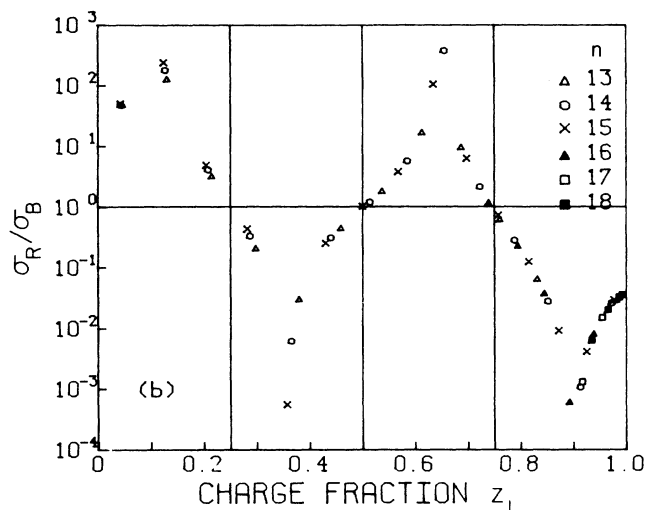

FIG. 8. Ratio of the cross sections given in Fig. 6 plotted as a function of Z_1 of the states.

There are two energy regions where attempts have been undertaken to study some aspect of these processes in hydrogen: above $E=0$ and near $E=-2\sqrt{F}$. We recently studied the region above $E=0$, and observed the asymmetry in the resonance profiles in a form of a blue wing.[15] In the lower-energy region, blue wings in low-lying $(n=4)$ states of hydrogen in a very large electric field $(\sim 3$ MV/cm), have been observed.[16] These asymmetries were much smaller than those in the energy region near $E=0$.

As the energy increases we find that above $E=0$ all states are already above their classical ionization limits. Variation of the ionization rate with energy becomes weak across the profile leading to symmetric profiles. Because of this and because the resonances become weak it is hard to examine these line-shape effects in this region in great accuracy. We should note that the shape of these broad resonances is basically the same in other atoms when a single quantum-defect channel is involved or dominates except for some common modulating energy-independent factor that depends on the quantum defect of the atoms.[6,17] The modulation factor is a result of the electron scattering from the electron core and it is equal to $\cos(2\pi\mu_l)$ where μ_l is the quantum defect; hence the core can only attenuate or perhaps invert these resonances with respect to those of hydrogen in this region. Recently Harmin derived analytical expressions for these asymmetric profiles in the form of Lorentzian profiles with an energy-dependent reduced width that depends on a single parameter.[18] His results indicate that the maximum derivation from Lorentzian profiles occur for resonances near the top of a barrier.

In here we examine the processes in a much favorable energy reigon which is somewhat away from the two limiting thresholds. The intermediate-energy region offers series of states that have large excitation cross sections over a reasonably wide range of energy. In addition it offers a wide range of gaps, both positive and negative, between the states and their classical ionization barrier.

We should note that this property is unique to hydrogen because in complex atoms the pairs (state and its ionization barrier) cannot be isolated because of scattering from the electronic core, leading to an autoionization region for the region above $E = E_{SP} = -2\sqrt{F}$, which is called a saddle point in the case of complex atoms. Strictly speaking this is not true even in hydrogen since relativistic effects which have not been included destroy the separability of the problem.[19] Such an effect, however, drops as n^{-3}; hence it becomes negligible for high n.[19,4] The scattering of the electron from the electronic core tends to coherently mix the excitation of the Stark states, thus preventing their selective excitation. Moreover, in the autoionization region, the ionization rate (width) of a long-lived state can be greatly increased if it is mixed with rapidly ionizing states. Such effects have recently been studied in He near the saddle point,[20] and the Stark theory has also been adapted to this region, thus allowing comparison between experiment and theory in He in this region.[21]

Figure 9 gives an enlargement of a portion of the spectrum given in Fig. 4(a). The states labeled by the quantum numbers (n_1, n_2), (16,0), (15,1), and (14,2), belong to the manifold $n = n_1 + n_2 + |m| + 1 = 17$. We observe for this manifold that as n_1 increases, the states get sharper. On the other hand, the states labeled by (15,1) and (15,0) have the same quantum number n_1 but belong to the two n manifolds 17 and 16, respectively. This series shows that for the same n_1 the states get wider as n increases. Table IV gives "the measured half widths at half maximums (HWHM)" of these states $\Gamma_e/2$ (see below). The table also gives the calculated HWHM $\Gamma/2$, location of the top of the barrier (classical ionization limit) E_c, and the gaps $E - E_c$ for all of the states given in Fig. 4(a). Because some of these states are highly asym-
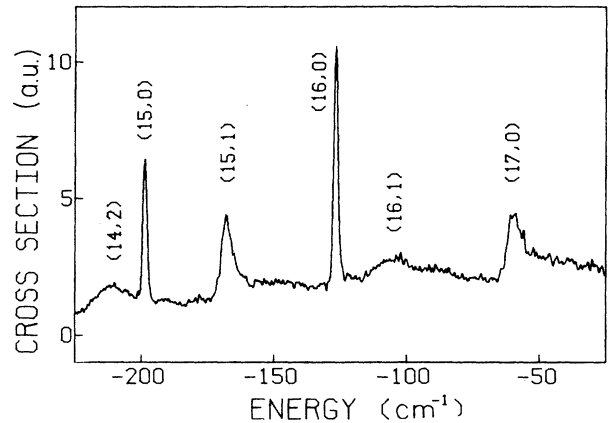

FIG. 9. Enlargement of a portion of the photoionization spectrum of the $m_l = 0$ blue state using π polarization and at field value of 16.8 kV/cm.

metric, we give two HWHM's for those, the HWHM on the red side of the resonance and the HWHM on the blue side of the line. Some of these wide asymmetric ones, however, overlap with other states thus preventing the measurement of both HWHM's; thus we enter only the one (red) which we can measure. There are three manifolds of states to be considered. Manifold one is composed of states (16,0), (15,1), and (14,2); manifold 2 is composed of states (15,0), (14,1), (13,2), (12,3), and (11,4); and manifold 3 is composed of states (13,1), (12,2), (11,3), and (10,4).

It is interesting to note that the position of each of the states of manifold 2, except for the last one, occur below the corresponding classical ionization limit (negative gap);

TABLE IV. Spectroscopic data on the $m_l = 0$ sharp Stark states excited from $n = 2$, $m_l = 0$ blue state. The states are shown in Fig. 4(a). The table gives the parabolic and principal quantum numbers, Z_1, the energy of the top of the barrier E_c, the energy gap $E - E_c$, the calculated and measured HWHM's $\Gamma/2$ and $\Gamma_e/2$. For highly asymmetric resonances we have two entries for the widths representing the HWHM's on the red and blue sides, unless we cannot measure both due to overlap with nearby states.

(n_1, n_2)	n	Z_1	E_c	$E - E_c$	$\Gamma/2$	$\Gamma_e/2$
17,0	18	0.991	−75.3	18.1	2.4,4.6	2.5[a]
16,1		0.964	−151.4	49.9	10.3[a]	9[a]
16,0	17	0.985	−96.3	−26.7	0.17	0.14
15,1		0.953	−172.6	5.5	1.7,2.6	2.1[a]
14,2		0.915	−231.8	22.7	5.7[a]	6.6[a]
15,0	16	0.98	−112.6	−83.8	3×10^{-4}	1.1×10^{-4}
14,1		0.937	−198.9	−36.2	0.022	0.016
13,2		0.89	−260.7	−13.5	0.27	0.23
12,3		0.844	−313.1	−0.5	1.2, 1.6	1.6, 2.5
11,4		0.79	−360.9	8.52	3.0	
13,i	15	0.924	−218.7	−96.3	5×10^{-6}	
12,2		0.870	−285.7	−63.9	10^{-4}	0.5×10^{-4}
11,3		0.814	−341.9	−42.4	4×10^{-3}	1.8×10^{-3}
10,4		0.756	−392.0	−27.1	0.03	0.032

[a]Unavailable half width because of overlap with other states.

hence they ionize via tunneling. Because of this their widths are quite small. But one can see that as the state gets closer to the top of the barrier, its width (ionization rate) increases drastically. Because of the limitation on our energy resolution, laser bandwidth, and inhomogeneity in the electric field, we cannot measure the true widths of those states directly. The third manifold of states also occur below their ionization limit, and display the large variations in width.

The first manifold of states occur closer to the top of the barrier, with state (16,0), being 26.7 cm^{-1} below, while states (15,1) and (14,2) lie at 5.5 and 22.7 cm^{-1} above. The calculated widths 0.16, 2.8, and 5.5 cm^{-1}, respectively, show large variation, being narrow below and quite wide above the barrier. The spectrum in Fig. 9 shows this effect.

Deconvolution of the spectra gives the "measured widths" of the states of manifold 1 which were given in Table IV. Although we cannot see the variation in the widths of very sharp tunneling states, we can "measure" their width if we use their calculated cross sections. Because they are much narrower than the instrumental width Γ_i, then their effective apparent experimental cross section is just $\sigma_e^{(c)} = \sigma \Gamma_e / \Gamma_i$. Using Γ_i and σ, we can find Γ_e. These are the ones given in Table IV. We find reasonable agreement between the calculated rates and the measured rates.

Table IV also shows the trend of the width of states of manifolds of same n_1, but different n. Unfortunately, in each n_1 manifold we have only two states with finite width and sufficient strength to be measurable. The numerical calculations show that indeed the width rises as n increases while keeping n_1 constant for all of the three n_1
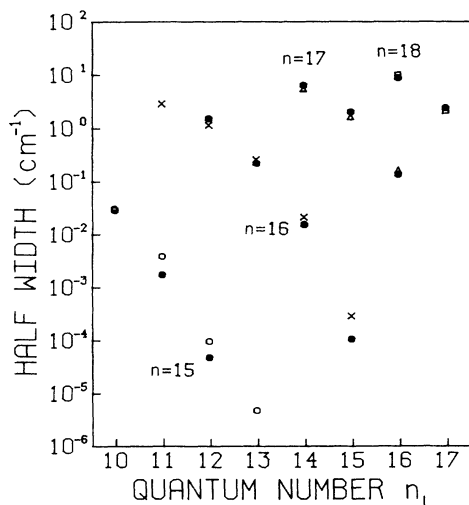

FIG. 11. Plots of the HWHM vs the principle quantum number n (for fixed n_1) of three Stark n_1 manifolds in the photoionization spectrum of the $m_l = 0$ state of $n = 2$ using π polarization and at 16.8 kV/cm. The same data is given in Table III. The open circles and the solid circles are those of the experiment and the exact numerical calculations. We used HWHM of the red wing of the wide asymmetric profiles.
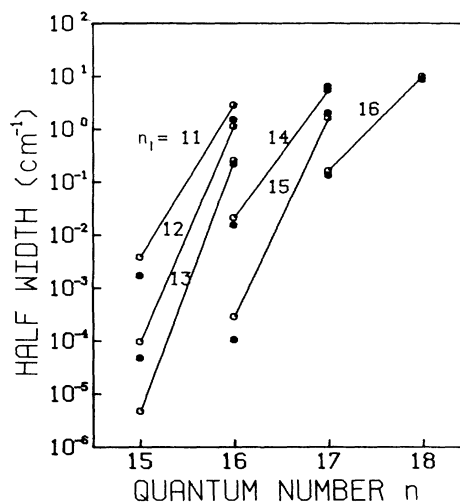
manifolds.

Figure 10 gives the measured width, and the exact numerical width as a function of n_1 (fixed n) for the three n manifolds. The n_1 axis is also the energy axis. Figure 11 gives the measured width and the exact numerical width as a function of n (fixed n_1) for the three n_1 manifolds.

A similar deconvolution process was applied to the spectrum of Fig. 4(b). The measured width agrees very well with the calculated one. Moreover, the results show that the dependence of the width on n_1 and n are the same as that of Figs. 10 and 11.

In conclusion, we have studied the ionization yield from single isolated channels in hydrogen in the presence of strong external electric fields. We have used selective excitation of appropriate charge distribution of initial excited states to either suppress or enhance the photoionization to a given final state, resulting in a great deal of simplification of the ionizing Stark spectrum. We have observed narrowing in the line shape as the quantum number n_1 increases (for fixed n) and broadening as n increases (for fixed n_1). Moreover, the ratio of the cross sections from the $m_l = 0$ blue states as a function of Z_1 is found to be universal for all states, and the Z_1 fractional changes of 0, $\frac{1}{4}$, $\frac{1}{2}$, $\frac{3}{4}$, and 1 demark regions where the ratio alternates between larger and smaller than one, respectively. Work is underway for studying mixing of channels caused by relativistic effects.[19]

ACKNOWLEDGMENTS

FIG. 10. Plots of the HWHM vs the parabolic quantum number n_1 (for fixed n) of three Stark n manifolds in the photoionization spectra of the $m_l = 0$ state of $n = 2$ using π polarization and at 16.8 kV/cm. The same data is given in Table III. The open angles and the solid circles are those of the experiment and the exact numerical calculations. We used the HWHM of the red wing of the wide asymmetric profiles.

*On leave from the University of Science and Technology of China, Beijing, People's Republic of China.

[1]See, for example, *Atomic Excitation and Recombination in External Fields*, edited by M. H. Nayfeh and C. Clark (Harwood Academic, New York, 1985).

[2]M. H. Nayfeh, Bull. Am. Phys. 29, 1489 (1984).

[3]Similar concentration has been observed by K. Welge (in Ref. 1).

[4]P. M. Koch and D. R. Mariani, Phys. Rev. Lett. 46, 1295 (1981); 41, 99 (1978).

[5]U. Fano, Phys. Rev. A 24, 619 (1981).

[6]D. A. Harmin, Phys. Rev. Lett. 49, 128 (1982); Phys. Rev. A 24, 2491 (1981); 26, 2656 (1982); 30, 2413 (1984).

[7]V. D. Kondratovich and V. N. Ostrovskii, Zh. Eksp. Teor. Fiz. 83, 1256 (1982) [Sov. Phys.—JETP 56, 719 (1982)]; 79, 395 (1980) [52, 198 (1980)].

[8]R. J. Damburg and V. V. Kolosov, J. Phys. B 9, 3149 (1976).

[9]E. Luc-Koenig and A. Bachelier, J. Phys. B 13, 743 (1980); 13, 1769 (1980); Phys. Rev. Lett. 43, 921 (1979).

[10]W. L. Glab, K. Ng, D. Yao, and M. H. Nayfeh, Phys. Rev. A 31, 3677 (1985).

[11]W. L. Glab and M. H. Nayfeh, Opt. Lett. 7, 380 (1982).

[12]K. H. Welge and H. Rottke, in *Laser Techniques in the Extreme Ultraviolet*, Proceedings of the Conference on Laser Techniques in the Extreme Ultraviolet, OSA, Boulder, Colorado, 1984, AIP Conf. Proc. No. 119, edited by S. E. Harris and T. B. Lucatorto (AIP, New York, 1984), pp. 213–219; in *Atomic Excitation and Recombination in External Fields*, edited by M. H. Nayfeh and C. Clark (Harwood Academic, New York, 1985).

[13]H. A. Bethe and E. E. Salpeter, *Quantum Mechanics of One-and-Two Electron Atoms* (Springer, Berlin, 1957).

[14]R. E. Langer, Phys. Rev. 51, 669 (1937).

[15]W. L. Glab and M. H. Nayfeh, Phys. Rev. A 31, 530 (1985).

[16]T. Bergeman, C. Harvey, K. Butterfield, H. C. Bryant, D. A. Clark, P. Gram, D. MacArther, M. Davies, J. Donahue, J. Dayton, and W. W. Smith, Phys. Rev. Lett. 53, 775 (1984).

[17]T. S. Luk, L. DiMauro, T. Bergeman, and H. Metcalf, Phys. Rev. Lett. 47, 83 (1981).

[18]D. A. Harmin, Phys. Rev. A 31, 2984 (1985).

[19]T. Bergeman, Phys. Rev. Lett. 52, 1685 (1984).

[20]W. Van de Water, D. Mariani, and P. M. Koch, Phys. Rev. A 30, 2399 (1984).

[21]D. A. Harmin, Phys. Rev. A 30, 2413 (1984).